The International Journal of Advanced Manufacturing Technology
https://doi.org/10.1007/s00170-025-15405-1

ORIGINAL ARTICLE

Statistical approach to determine cutting conditions and cutting geometry for edge trimming of G/PA12 plates

Petr Masek[1] · Jaroslav Kovalcik[2] · Pavel Zeman[1]

Received: 31 October 2024 / Accepted: 11 March 2025

Abstract

Glass-fibre-reinforced polyamide 12 (G/PA12) composite, a material with considerable potential in the automotive industry, poses notable machining challenges owing to its low glass transition temperature, low matrix stiffness, and the abrasive nature of the glass fibres. Although near-net-shape manufacturing processes minimize excess material, the free edges often require precise trimming to achieve the specified product accuracy and quality. In this study, optimal cutting conditions and tool geometries for edge trimming of G/PA12 composite plates were investigated. A two-stage experimental design was adopted, beginning with the identification of principal control factors using a standard polycrystalline diamond (PCD) cutter. These findings were subsequently compared with results obtained using various double-helix cutter geometries. Double helix cutters have demonstrated significant improvements in surface quality, achieving up to 100 times improvement with a 20% reduction in temperature and only a slight increase in resultant force. An elevated feed per tooth rate was shown to further enhance surface quality, although at the cost of higher cutting forces. A highly accurate cutting force model was formulated, explicitly accounting for both rake angle and helix effects. Temperature measurements obtained with an infrared camera and based on experimentally determined emissivity values revealed that the glass transition temperature was consistently exceeded; however, the melting point was not exceeded.

Keywords Composites with thermoplastic matrix · Edge trimming · Temperature · Delamination · Cutting forces · Cutting tool geometry

Nomenclatures

G/PA12	Glass/Polyamide12 composite
PCD	Polycrystalline diamond
CVD-D	Chemical vapour deposited diamond
T_g	Glass transition temperature
E_x	Young's modulus in axis X
E_y	Young's modulus in axis X
G_{xy}	Shear modulus
RH	Relative humidity
F	Resultant force
F_x	Force in axis X
F_y	Force in axis Y
F_z	Force in axis Z
F_c	Cutting force
F_f	Feed force
F_a	Active force
F_p	Passive force
ADL	Averaged delamination length
f_t	Feed per tooth
v_c	Cutting speed
a_e	Radial depth of cut
M	Radiant exitance
ε	Emissivity of grey object
T	Temperature
σ	Stefan-Bolzmann constant
$k_{c1,1}$	Specific cutting force $h = b = 1$
m_c	Chip thickness coefficient
h_D	Chip thickness
b_D	Chip width
γ	Rake angle
λ	Helix angle
K_{gl}	Modification factor for geometry

✉ Petr Masek
P.Masek@rcmt.cvut.cz

[1] Department of Production Machines and Equipment, Faculty of Mechanical Engineering, Center of Advanced Aerospace Technology, Czech Technical University in Prague, Technicka 4, 16607 Prague 6, Czech Republic

[2] Department of Production Machines and Equipment, Faculty of Mechanical Engineering, Czech Technical University in Prague, Technicka 4, 16607 Prague 6, Czech Republic

Published online: 20 March 2025

A, B, C	Coefficient of cutting geometry
DF	Degrees of freedom (ANOVA test)
Adj MS	Adjusted Mean Square (ANOVA test)
Adj SS	Adjusted Sum of Squares (ANOVA test)

1 Introduction

Composite materials are heterogeneous materials made of two or more components, where each component has very different mechanical and physical properties from the others. Composites contain reinforcement, an internal support structure, and a matrix that binds the reinforcement together. Matrices are usually much softer, tougher, and their tensile strength is several times lower than that of reinforcements [1]. Both the reinforcement and the matrix can be composed of various materials. Their appropriate combination and the method of depositing the reinforcement in the matrix give composites their unique properties, which are in high demand. Their excellent strength-to-weight ratio is used in the aeronautical or aerospace industry [2, 3], and they are also very popular in the automotive, defence [4] or sports industries [5]. Matrices can be made of metal, ceramic or polymer [6]. This study is focused on polymer matrices. Polymers used in composite materials can be thermosets or thermoplastics. Thermosets are heat-curable and cannot be heat-moulded. The main representatives of thermosets are epoxy and polyester resins. Thermoplastic can be shaped with heat. The most well-known thermoplastic polyamides (PA6, PA12), PET, PEEK, PEKK, etc. Reinforcement for polymer matrices can be glass, carbon, polymer or natural. The reinforcement typically takes the form of fibres, which can be short, long or continuous, loose or woven [7].

Properties given by the combination of matrix and reinforcement and its internal structure give composites different machinability. Composites are typically produced in a near-net-shape, but in order to obtain a product of the required dimensions, it is necessary to process functional surfaces, holes for joining or simple trim the free edges of the composite workpiece. [7]. Composites with resin matrices usually have worse machinability than those with thermoplastic matrix. The reason is the brittle fracture of the matrix and dust-like chips generated during machining [8]. On the other hand, there is a risk that the thermoplastic matrix will soften during high temperature and the melted matrix may create build-up or permanently clog the cutter flute [9]. In principle, composites are not recommended to be machined under coolant. However, the application of minimum quantity lubrication (MQL) or an emulsion can help reduce cutting forces [10]. Therefore, different types of cutting tools are recommended for both types of dies [11, 12]. Both types of matrices lead to different suitable machining approaches. This study focuses on thermoplastic composite materials.

The reinforcement in fibre composites is very strong and hard. Because of this, these fibres are very abrasive, and tool life is very short when using standard cutting material such as high-speed steel or tungsten carbide [13]. Therefore, the recommended cutting material is polycrystalline diamonds (PCD) or chemical vapor deposition diamonds (CVD-D) or their thin layers on tungsten carbide substrates [6, 7]. This study deals with the influence of cutting conditions and cutting geometry on the resulting composite behaviour and the influence of tool wear on temperature, forces and quality of the machined surface is suppressed by the choice of PCD or CVD-D cutting materials for the tools. Glass fibre undergoes brittle deformation, similar to carbon fibre [14, 15]. Fibers can produce dust particles that may be respirable [7, 16]. A smaller volume of these particles can be observed in fibre-reinforced thermoplastic composites (FRTCs) because they tend to form regular chips that are able to bind broken fibres. This risk is much lower than with thermoset composites but is still present. And for this reason, it is necessary to vacuum them to avoid harm to the operator [17, 18].

A fundamental quality problem caused by the machining process is delamination of composites. Delamination is the separation of adjacent layers of the composite [19]. Delamination is caused by forces, their magnitude and direction acting against the fibre orientation. The magnitude and direction of these forces are determined by the geometry of the cutting tool and cutting conditions, as demonstrated by He et al. [20] in his studies. Relationship between process parameters and delamination and forces was studied in the meta-study of Patel et al. [21]. Hintze et al. [22] studied the influence of the tilting and helix of a cutting tool on delamination and showed how to reduce delamination in both up-milling and down-milling processes. Davim et al. dealt with the statistical evaluation of cutting parameters to obtain their significance in the milling of CFRP materials. Davim found that the feed rate was the most influential parameter for the delamination factor *Fd*, surface roughness and accuracy [23, 24]. Feed per tooth was identified as an easily adjustable control factor with a significant influence on the CFRP cutting process, however, its correct selection and to keep it is essential [25]. How to maintain consistent feed was solved, for example, by Vavruska et al. [26]. For different cutters, Praveen et al. presented different effects of cutting parameters on the quality of the machined surface. In this case, the geometry of the cutting tool probably had a big influence [27]. In their study, Jenartharan and Naresh evaluated data combining cutting tool geometry and cutting parameters. The effect of cutting parameters was higher than the helix angle, but the fibre orientation had the greatest effect on delamination [28]. In another study, fuzzy logic was used to optimize cutting parameters for GFRP milling [29]. Although some effects may be similar for a group of certain materials, it is not possible to identify them for all types of composite materials, due to their possible variations. For G/PA12, which is the subject of this study, there has not yet been an analysis of the effect of cutting geometries and cutting conditions on the quality of the machined surface.

The favourable effect of a positive rake angle and a higher clearance angle on the surface quality was experimentally carried out by Vos et al. [30]. A numerical analysis of the results obtained during orthogonal machining confirmed that a larger face angle had a positive effect on reducing the cutting force and damage of the CFRP composite [31]. Similar results were obtained by Sheikh-Ahmad et al. during milling of UD-CFRP, showing that a positive rake angle reduces forces [32]. Chatelain and Zaghbani et al. tested special cutting tool geometries for milling composite materials. The compression geometry was less stable than other geometries tested but had a positive effect on thrust force [33]. Su determined a specific cutting force model and determined its coefficient for plain-woven CFRP using the Standard mechanistic model [34]. Kala et al. [35] used another approach to determine a specific shear coefficient. They applied the Mechanistic Model presented earlier by Altintas [36] and neural networks on C/Epoxy composite. Karpat [37] also used a mechanistic model, but he developed it specifically for the geometry of a double helix cutter. In our previous work, this approach was improved by considering the axial positions of the cutting tool relative to the machined surface on C/PPS [38]. Determining a predictive model for force effects helps in selecting appropriate cutting conditions and cutting geometry. However, these force effects will vary for different composite types and have not been investigated for G/PA12.

Composite materials with polymer matrix are relatively less resistant to high temperatures. Accordingly, the effect of cutting conditions on temperature has been studied several times for various polymer composites. Rahman found that while milling the C/PEEK composite, the glass transition temperature (T_g) of the matrix was exceeded at a cutting speed of 75 m/min. In this study, the melting point was not reached, and the maximum temperature was lower than 250 °C at a relatively high cutting speed of 200 m/min [18]. Kerrigan used an integrated sensor in the cutting tool when milling C/epoxy and found that the cutting speed was less affected. Nevertheless, workpiece thickness was identified as the most significant controlling factor in this experiment [39]. Yoshiro et al. measured the temperature in a full section of CFRP using three different methods (infrared camera, embedded thermocouple, and tool-workpiece thermocouple). The cutting speed was increased up to 300 m/min, at which point the glass transition temperature was reached. However, this cutting speed was recommended as the matrix was not affected [40]. Jia et al. also used an embedded thermocouple during CFRP milling under cryogenic coolant. Liquid nitrogen was able to reduce the temperature from 135 °C to – 50 °C [41]. In our previous study, the temperature of C/PPS was measured with a semi-artificial thermocouple. In addition, cutting speed was identified as the most influencing control factor. The glass transition temperature was reached in all measurements, but the melting point was not. Thus, the cutting speed could be increased to achieve higher productivity [38]. For G/PA12, which has a low glass transition temperature or melting point, careful selection of cutting conditions will be necessary, the limits of which are not yet known.

Despite the relatively large number of scientific publications on the subject of composite materials processing, there is only a limited number of them that deal with the milling of thermoplastic composites with fibre reinforcement. Within this group of materials, there are also many variations in the combination of matrix and reinforcement, which leads to a large number of different mechanical properties and technological properties of the composites, such as machinability. The G/PA12 composite has not been studied from this point of view. The low glass transition temperature of the matrix, coupled with the high abrasiveness of the glass fibre reinforcement in G/PA12 composites, poses substantial machining challenges, making the selection of appropriate cutting conditions and tool geometry paramount for achieving high-quality machined surfaces. This study seeks to advance the understanding of G/PA12 machinability by identifying optimal cutting parameters and tool geometries that minimize cutting forces, maintain safe operating temperatures, and yield superior surface finishes. A primary contribution is the development of a predictive cutting force model and a validated temperature measurement methodology, both specifically tailored to this challenging material. A two-stage experimental design—employing standard polycrystalline diamond (PCD) as well as double-helix cutting tools—was implemented to systematically investigate critical control factors and elucidate the effects of cutting geometry.

2 Materials and method

2.1 G/PA12 composite

The composite material was polyamide 12, reinforced with glass fibres (G/PA12). The matrix was a semi-crystalline engineering thermoplastic, commonly used in the automotive industry. The glass fibre was of EC11 type with improved tensile strength stability. The reinforcement had a 4H satin woven structure. The plate had a thickness of 3 mm. Other specifications of the G/PA12 are provided in Table 1.

Table 1 Material properties of the G/PA12

Property	Unit	value
Ply thickness	mm	0.375
Reinforcement		
Ply orientation	[[(0,90)/(±45)]4]s	
Tensile strength	MPa	1900
Elongation	%	3.7
Tensile strength modulus	GPa	73
Density	g/cm^3	2.65
Matrix		
Polymer volume in composite	%	50
Glass transition temperature	°C	50
Melting point	°C	170
Chemical resistance		good
Moisture uptake *23 °C, 50% RH*	%	1.5
Mechanical properties of composite (bending)		
Ex	MPa	59,000
Ey	MPa	43,000
Gxy	MPa	4428

The G/PA12 samples were prepared in dimensions 40×70 mm. The samples were clamped in a fixture which was bolted to a Kistler 9255B dynamometer. This fixture allowed to clamp up to 4 specimens at once.

2.2 Machine tool and equipment

The machine tool was a 3-axis CNC machining centre with linear drives on each axis. The maximum axis acceleration was 20 m/s^2. The maximum spindle speed was 15,000 rpm and the spindle power was 18 kW (Fig. 1a).

Cutting forces were measured using Kistler dynamometers 9255B and 9123C (Fig. 1d). The9255B Kistler dynamometer was used for main comparison of the control factors. Measured force components were F_x, F_y and F_z. From these components, the resultant cutting force F was calculated according to Eq. (1) [42].

$$F^2 = F_a^2 + F_p^2 = F_c^2 + F_f^2 + F_p^2 = F_x^2 + F_y^2 + F_z^2 \tag{1}$$

where F_p is the passive force and was equal to F_z measured by the dynamometer. F_a is the active force which in this case is calculated as the vector sum of the forces F_x and F_y measured by the dynamometer. F_a can be also defined by the cutting force F_c and the feed force F_f. The 9123C rotary dynamometer was used to describe the coefficient of tangential specific cutting force for different double-helix cutting tools with CVD-D coating.

The surface quality was evaluated by the average delamination length (*ADL*, a method previously employed in our earlier study [38]). This method requires taking a photo of each side of the machined surface (bottom, front and top), see Fig. 1b. The resulting delamination areas were calculated

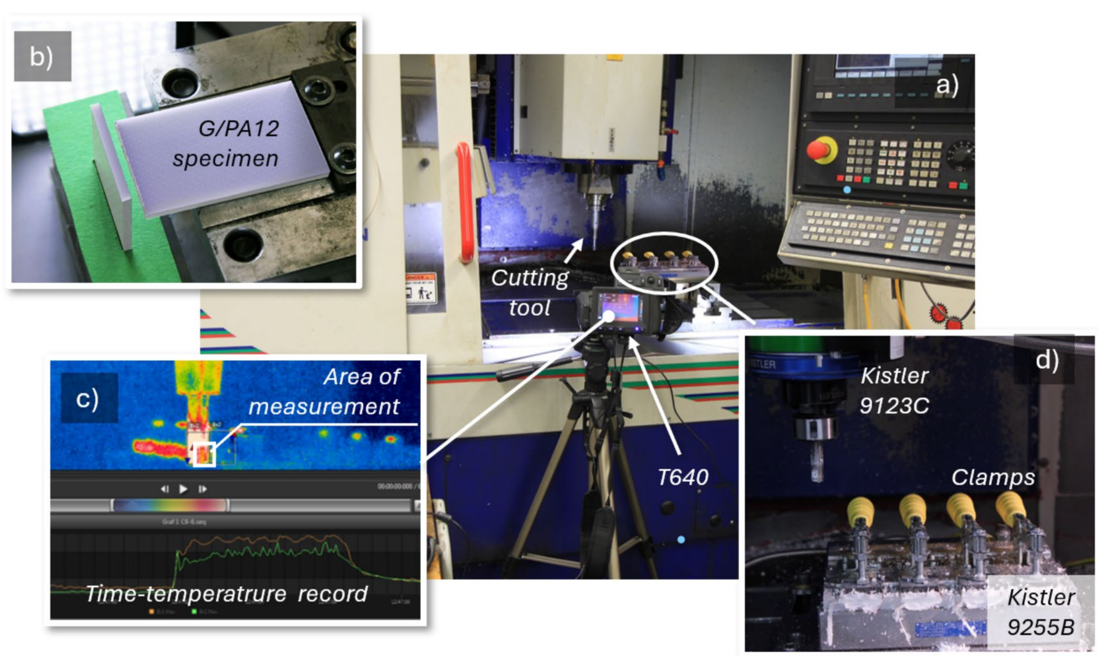

Fig. 1 Experimental setup: (**a**) MCFV 5050 LN CNC machine tool, (**b**) photography arrangement for delamination measurement, (**c**) temperature field measurement, and (**d**) force measurement setup

as the average sum of squares, accounting for the burr's deviation from the machining plane as depicted in Fig. 2 and described by Eq. (2). The photos of burrs were taken using Canon Eos 550D and the magnification of surfaces were taken using microscope LIM.

$$ADL = ADL_{top} + ADL_{bottom} = \frac{\sqrt{\left(A_{top1}^2 + A_{top2}^2\right)}}{l} + \frac{\sqrt{\left(A_{bottom1}^2 + A_{bottom2}^2\right)}}{l} \tag{2}$$

For the experimental evaluation, the method of temperature measurement from the thermal area measured by an infrared camera was used. This method was the only option for measuring thin plates made of electrically non-conductive composites, in which it is not possible to place a thermocouple. There are certain limitations with this type of measurement, such as the emissivity of the measured objects, the response speed of the IR sensor, the limited field of view of the infrared camera or the resolution of the IR sensor. The temperature was measured with a Flir T640 infrared camera. This camera was able to measure continuously at 30 Hz with an accuracy of 2 °C. The monitored area encompassed the machined surface adjacent to the cutting tool, observed from a distance of 0.75 m. (Fig. 1c).

2.3 Cutting tools

A standard catalogue PCD tool with a diameter of 12 mm was used for preliminary experiments (Fig. 3). This cutting tool has two PCD diamond cutting edges brazed onto a tungsten carbide body. The angle of the rake of the cutting tool was 0° and the clearance angle was 10°, the tilting of the PCD element was 2°.

The main block of the experiment was performed with 4 non-standard cutting tools with double helix compression geometry and 5 cutting edges. The face angle and helix varied for each cutting tool (Table 2). The clearance angle was the same (12°) for all cutters.

2.4 Cutting conditions

The preliminary experiment was carried out to determine the significance of the basic cutting conditions. Different cutting conditions were tested in a full factorial design of experiment (Table 3). The most significant factor for a given measurement was planned to be a comparison factor for the second block of experiments.

The second block of the experiment was based on the results of the preliminary experiments. The basic problem was the completely different geometry of the cutting tool, which could affect the results. On the other hand, the preliminary experiments helped to adjust the boundary conditions and reduce the number of experiments needed for the main block. The main block consists of the most significant

Fig. 3 Standard PCD cutter PKD FRAESER 05492–12,000

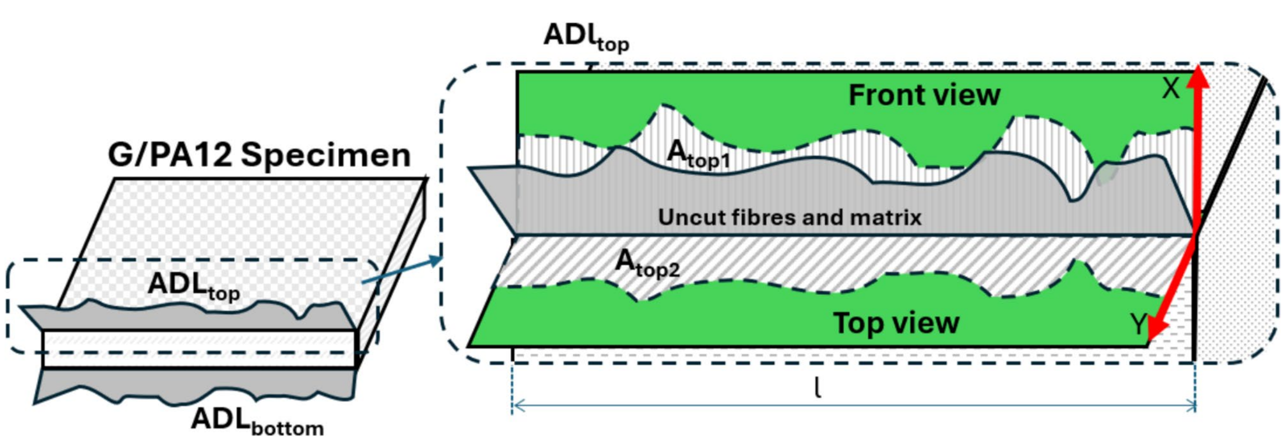

Fig. 2 Evaluation of delamination principles

Table 2 Tested compress cutters with various tool geometry

Cutting tool		Rake angle [°]	Helix angle [°]
R25H15		25	15
R25H5		25	5
R15H15		15	15
R15H5		15	5

Table 3 Cutting condition used for preliminary experiments with PCD cutter

Factor	Units	Symbol	Levels	
			1	2
Feed per tooth	mm	f_t	0.05	0.1
Cutting speed	m/min	v_c	100	300
Radial depth of cut	mm	a_e	1	3

Table 4 Cutting conditions used for testing double-helix cutters

Factor	Units	Symbol	Levels	
			1	2
Cutting speed	m/min	v_c	100	300
Feed per tooth	mm	f_t	0.05	0.15
Radial depth of cut	mm	a_e	1	3
Helix angle	°	λ	5	15
Rake angle	°	γ	15	25

control factor from the preliminary experiments and the geometry of the cutting tool, see the design of the experiment in Table 4. This comparison provided information whether the change in the cutting geometry had a more significant effect than the change in the selected control factor of the cutting conditions. Two levels were selected based on preliminary experimentation and reflected the recommended cutting conditions for comparable tools. Variations in cutting geometry were introduced to induce relatively substantial differences in outcomes, drawing on prior experience gained from machining various composite materials.

A full factorial design with replication was used for all experiments. The Results were compared using analysis of variance (ANOVA). When the data met the assumptions for parametric tests, ANOVA was used. In other cases, a non-parametric test was used. The results revealed significant control factors in the experiment.

3 Results and discussion

3.1 Emissivity of G/PA12

Emissivity was one of the key parameters important for correct temperature readings during machining tests. The emissivity was determined experimentally in an electric oven, where the G/PA12 sample was heated to 150 °C. Natural cooling was observed using a FLIR PM675 infrared camera, while the ambient and G/PA12 temperatures were measured. These data were compared and evaluated to determine the true emissivity of the composite.

The temperature in the vicinity of the area was measured by a thermocouple K and the ambient temperature was measured with a PT100 thermocouple (Fig. 4a) and recorded using an Almemo 5690–2 data logger. Heat was generated in an electric furnace and the natural cooling process was monitored at spot Sp1 with an infrared camera (Fig. 4b). The preset emissivity was 0.96. The cooling curves measured by the K-type thermocouple and the infrared camera were not the identical, indicating that the preset emissivity was incorrect. However, the curves showed a similar trend (Fig. 4c). The emissivity estimate for G/PA12 was calculated using the Stefan-Boltzmann law [43].

$$M = \varepsilon \sigma T^4 [Wm^{-2}] \quad (3)$$

Here ε was the emissivity of the given grey object, σ was the Stephan-Bolzman constant $5.67 \cdot 10.^{-8}$

WM^{-2} K^{-4} and T was the thermodynamic temperature [K]. According to Eq. (4) and the measured data, the average from the calculated emissivity values for

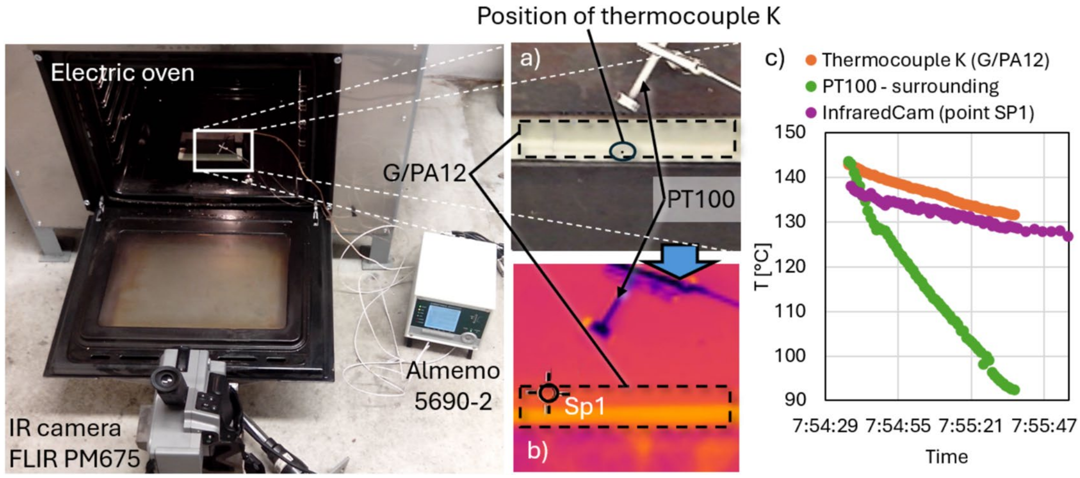

Fig. 4 Experimental investigation of the G/PA12 emissivity in electric oven: (**a**) composite placement, (**b**) infrared photograph of the same place, (**c**) recording of measurement

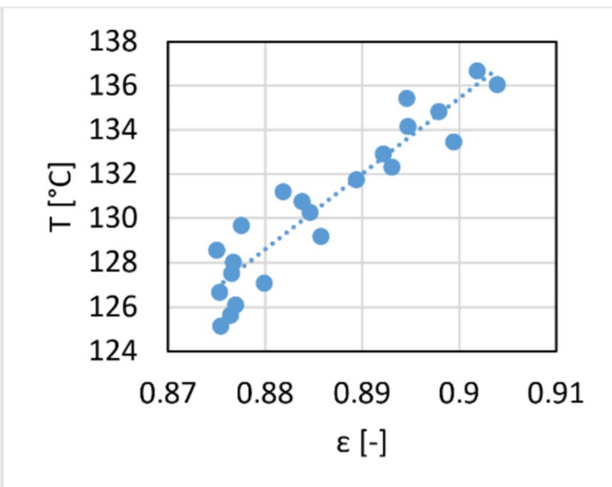

Fig. 5 Emissivity evaluation dependent on the temperature

the selected temperature range was estimated as 0.89 (Fig. 5). This value was the input value for all temperature measurements.

$$\varepsilon_1 T_1^4 = \varepsilon_2 T_2^4 \tag{4}$$

ε_1 was the preset emissivity, T_1 was the temperature measured by the infrared camera, T_2 was the temperature measured by the thermocouple K. ε_2 was the emissivity to be calculated.

3.2 Cutting forces

The PCD cutting tool was used in the preliminary experiment. Cutting conditions were used from Table 3. The calculated resultant forces reached up to 75 N when the chip thickness was the highest. Machining was stable with no audible chatter under all cutting conditions. After machining, the collected data were statistically tested for the possibility of using the ANOVA test. The ANOVA test could not be used because the condition of the normality for the data was not met. The non-parametric Kruskal–Wallis test was used instead. The Kruskal–Wallis test for the resulting cutting force revealed a significant influence of the control factors f_t and a_e (Fig. 6). The p-value of these two factors was less than the chosen significance level, which means that the medians of the two levels were different. All measured factors increased with increasing level of factor.

Both tested parameters f_t and a_e were statistically significant also in comparison with the cutting geometry, see Fig. 7a and b. The main effect plot in this case revealed that the higher the factor was, the higher was the measured evaluated forces. That made sense because the chip area increased with these two parameters. However, they were much dominant then the rake and helix angle which decreased the force when were higher. The rake angle changes the direction of the force and affects the size of the primary cutting zone, generally resulting in a lower cutting force. The fibres bend less and also compress the matrix less in the primary cutting zone. As a result, less energy accumulates in the cutting zone, which has a positive effect on cutting forces. The helix angle increased the smoothness of the cutting edge engage and that could have positive effect on cutting force as well.

Here, **DF** (degrees of freedom) is determined as the number of levels minus one. The Adj SS denotes the portion

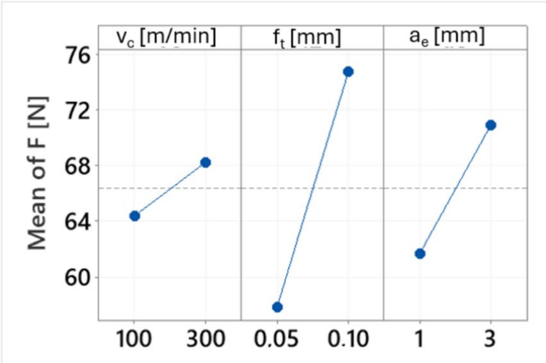

Descriptive Statistics						Test	
	Source	n	Median	Mean Rank	Z Value	H Value	P Value
v_c	100	12	62.3309	11.6	-0.64	0.40	0.525
	300	12	69.3384	13.4	0.64		
	Overall	24		12.5			
f_t	0.05	12	59.9355	6.8	-3.93	15.41	**0.000**
	0.10	12	76.3386	18.2	3.93		
	Overall	24		12.5			
a_e	1	12	60.3990	9.5	-2.08	4.32	**0.038**
	3	12	69.3825	15.5	2.08		
	Overall	24		12.5			

Fig. 6 Investigation of control factor via Kruskal–Wallis and Main effect plot for cutting conditions control factors and *F*

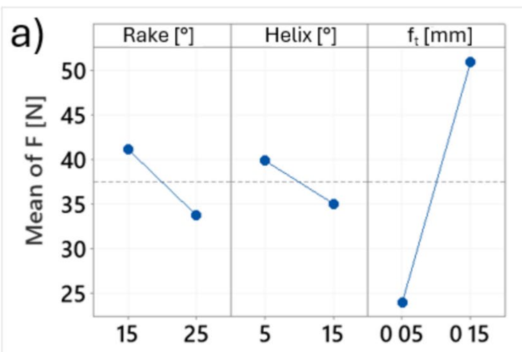

Source	DF	Adj SS	Adj MS	F-Value	P-Value
Helix	1	46.99	46.99	2.32	0.202
Rake	1	108.85	108.85	5.37	0.081
f_t	1	1445.6	1445.6	71.38	**0.001**
Error	4	81.01	20.25		
Total	7	1682.44			

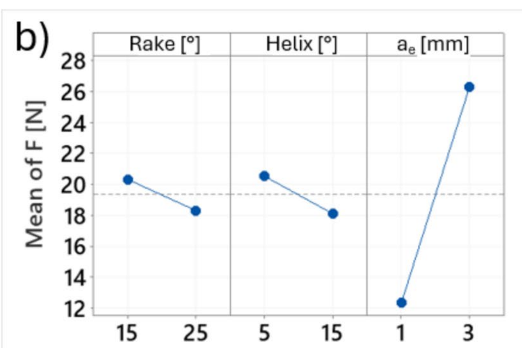

Source	DF	Adj SS	Adj MS	F-Value	P-Value
Helix	1	8.082	8.082	4.53	0.100
Rake	1	11.876	11.876	6.65	0.061
a_e	1	388.94	388.94	217.9	**0.000**
Error	4	7.140	1.785		
Total	7	416.037			

Fig. 7 Investigation of control factor via ANOVA and Main effect plot for *F* and: (a) f_t (v_c = 100 m/min, a_e = 3 mm) and parameters of geometry and (b) a_e (v_c = 100 m/min, f_t = 0.05 mm) and parameters of geometry

of the variation in the dependent variable that is explained by the model. The **Adj MS** represents the mean variation explained by the model and is calculated as Adj SS divided by DF. The response of the *F* to change in feed per tooth was predictable. Similar test with similar results were measured by Davim [24] or Sorrentino [44], for example. For this reason, the cutting force model was created based on control factor f_t.

A direct comparison of all tested cutters revealed higher resultant forces generated by the PCD cutter (Fig. 8) due to the geometry of the rake and the helix. A less positive rake face geometry caused higher resistance to cutting edge engagement and led to higher deformations and forces. A similar effect of rake angle was observed with double-helix cutters. The higher helix angle contributed to easier cutting edge engagement and thus further reduced forces.

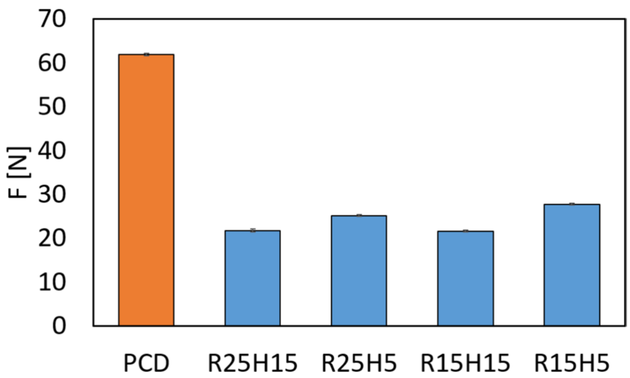

Fig. 8 Direct comparison of the resultant force for the tested cutter types under the cutting conditions: $a_e=3$ mm, $f_t=0.05$ mm, $v_c=100$ m/min

3.2.1 Cutting force model

A cutting model for G/PA12 and double-helix cutter was developed based on the Kienzle model. This experiment was designed separately from the main experiment because it required a higher number of levels to establish a reliable dependence of average chip thickness (h_D) on cutting force (F_c). This experiment was conducted with a rotary dynamometer Kistler 9123C. The advantage of this device is the ability to collect both tangential and radial cutting force data. The tangential component is essential to determine the Kienzle model. The f_t levels were set at 0.05, 0.07, 0.1, 0.13, 0.15 mm. Cutting speed and radial depth of cut remained constant at: $v_c=100$ m/min and $a_e=3$ mm. The h_D as well as average chip width (b_D) were calculated for each f_t.

The basic model Eq. (5) was derived from the Kienzle model:

$$F_c = k_c A_D = k_{c1.1} {h_D}^{1-m_c} b_D \tag{5}$$

where k_c is the specific cutting force. A_D is the average chip area. The coefficient $k_{c1.1}$ is the specific cutting force for $h=b=1$ mm, where both the face angle and helix angle are equal to 0 [N/mm^2]. The coefficient m_c expresses the effect of the thickness of the cut layer on the cutting force, respectively to the specific cutting force, and is dimensionless. This model Eq. (6) has been adjusted due to the helix and rake angle:

$$F_c = k_{c1.1} {h_D}^{1-m_c} b_D K_{gl} \tag{6}$$

The K_{gl} factor modifies the basic relationship due to the influence of the rake angle and the helix angle. In addition to these parameters, their interaction is also considered.

$$K_{gl} = 1 + A\gamma + B\lambda + C\gamma\lambda \tag{7}$$

The extended relationship for calculating the cutting force with the influence of the angle of the face and helix is:

$$F_c = k_{c1.1} {h_D}^{1-m_c} b_D (1 + A\gamma + B\lambda + C\gamma\lambda) \tag{8}$$

The coefficient A represents the effect of the face angle on the cutting force. The coefficient B represents the effect of the helix angle on the cutting force and the coefficient C represents the effect of the interaction between the face angle and the helix on the cutting force. The coefficient values were estimated by nonlinear regression in the Minitab SW program.

According to the p-value, all estimated coefficients, including the interaction between the helix and face angle, are statistically significant (Table 5). The coefficients from Table 5 can be directly substituted into Eq. (8), resulting in Eq. (9):

$$F_c = 101.856 h_D^{1-0.269} b_D (1 - 0.0259\gamma - 0.0451 l + 0.0022\gamma) \tag{9}$$

This model equation has a very high coefficient of determination, $R^2=0.994$. The scatter plot (Fig. 9) illustrates the correspondence between the measured and predicted data.

Table 5 Calculated coefficients for the cutting force model

Parameter	Coefficient	p-value
$k_{c1,1}$	101.856	1.2278E-13
m_c	0.269	8.9735E-10
A	−0.0259	1.5191E-08
B	−0.0451	6.6817E-08
C	0.0022	2.0583E-07

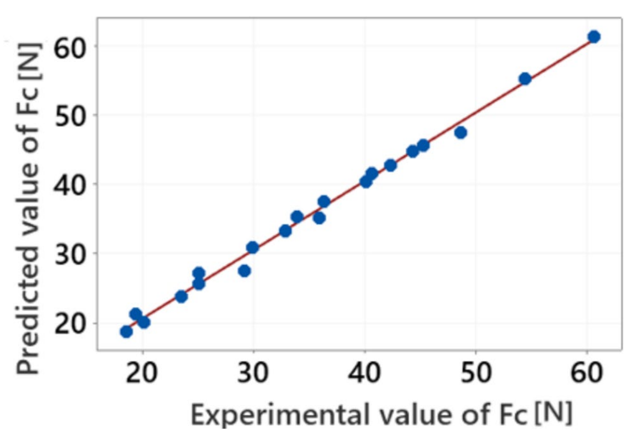

Fig. 9 Scatter plot for the cutting force model

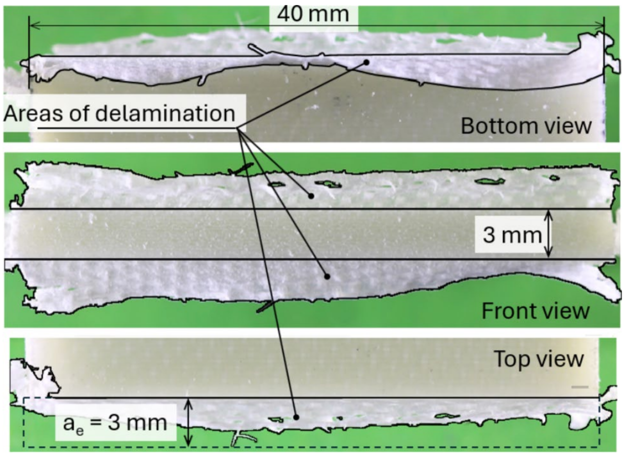

Fig. 10 Photography of delamination appeared during milling with PCD cutter

3.3 Delamination

Delamination of G/PA12 manifested as uncut fibres and matrix. In the case of the PCD cutter, the cutter was unable to cut the bottom and top burrs at all (Fig. 10). The ANOVA test of preliminary experiment showed that the a_e was the only statistically significant control factor. This finding numerically supports the mentioned hypothesis about the unsuitability of the PCD cutter for finishing the machined surface, see Fig. 11. The results of the preliminary delamination test did not identify any control factor for the next experimental phase, for this reason. All control factors had to be included in the next experiment. To reduce the number of tests, a separate experimental design was used for each factor, rather than a full factorial design.

The machined surface of G/PA12 showed uncut burrs along the edges of the composite sample and, to a small extent, pulled fibres from the surface, see Fig. 12. The low glass transition temperature of the matrix and its surface ductility probably limited signs of fibre pull-out. An initial assessment at the quality of the machined surface revealed a very high effect of f_t. The volume and number of free fibres appeared to be less for higher f_t, see Table 6. An analytical assessment of *ADL* confirmed this result. The difference between the two different cutting speeds or two different radial depths of cut was not noticeable upon initial inspection of the cut edge. If the cutter is able to cut the top and bottom layers, then the decisive value for the average

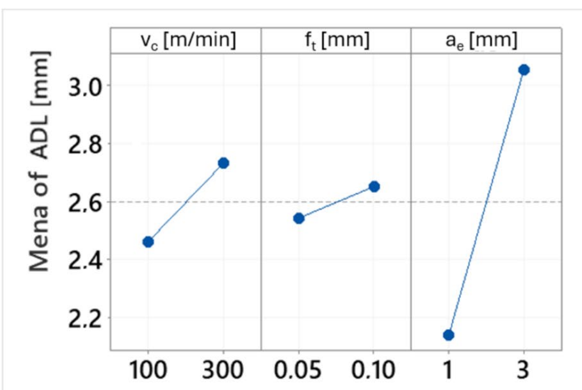

Source	DF	Adj SS	Adj MS	F-Value	P-Value
v_c	1	0.29024	0.29024	3.51	0.085
f_t	1	0.04725	0.04725	0.57	0.464
a_e	1	3.34118	3.34118	40.42	**0.000**
Error	12	0.99189	0.08266		
Lack-of-Fit	4	0.26893	0.06723	0.74	0.588
Pure Error	8	0.72296	0.09037		
Total	15	4.67057			

Fig. 11 Investigation of control factor via ANOVA and Main effect plot for cutting conditions control factors

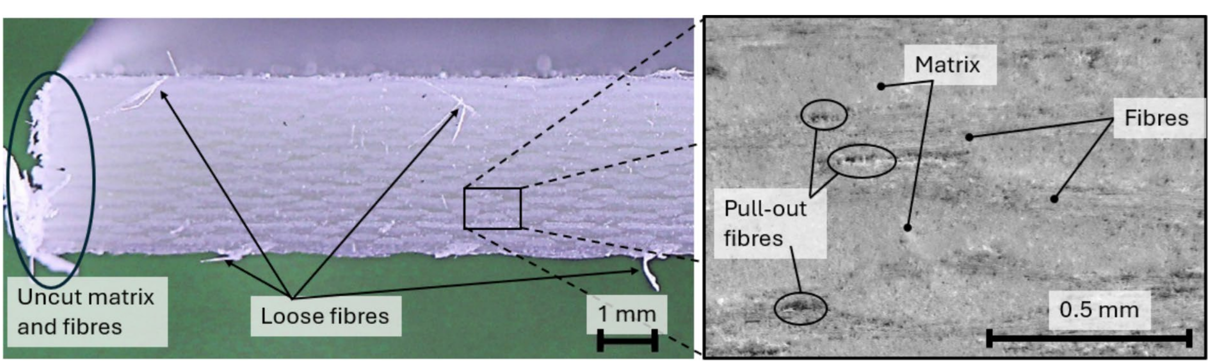

Fig. 12 An example of surface quality made by R25H15 (v_c = 100 m/min, f_t = 0.05, a_e = 3 mm)

Table 6 Comparison of delamination – an example for cutting tool R25H15

a_e = 3 mm; v_c = 100 m/min	a_e = 3 mm; f_t = 0.05 mm	v_c = 100 m/min; f_t = 0.15 mm
f_t = 0.05 mm	v_c = 100 m/min	a_e= 1 mm
	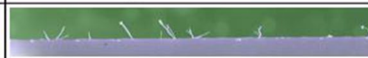	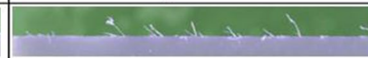
f_t = 0.15 mm	v_c= 300 m/min	a_e= 3 mm
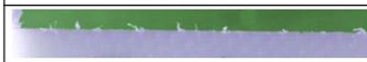	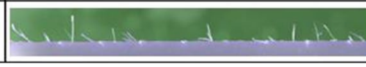	

delamination length is the minimum chip thickness associated with the high elasticity of the machined surface and the actual position of the cutting edge relative to the fibres during cutting. In this case, some loose fibres were bent rather than cut. A higher f_t reduces the probability of this happening.

A comparison of three cutting condition control factors and two cutting geometry control factors of double-helix cutters revealed that the f_t was statistically significant. Other factors were less significant compared to the cutting geometry control factors, based on a significance level of 0.05. This evaluation supported the estimate shown in Fig. 13a. The

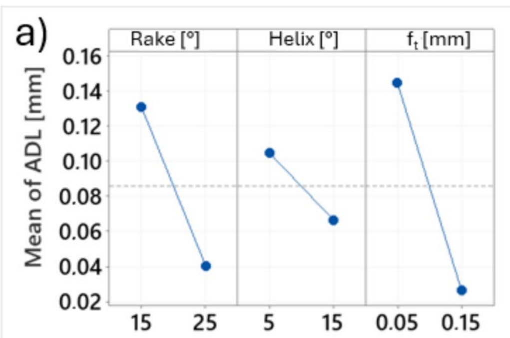

Source	DF	Adj SS	Adj MS	F-Value	P-Value
rake	1	0.01636	0.01636	4.80	0.093
helix	1	0.00289	0.00289	0.85	0.409
f_t	1	0.02791	0.02791	8.19	**0.046**
Error	4	0.01362	0.00340		
Total	7	0.06079			

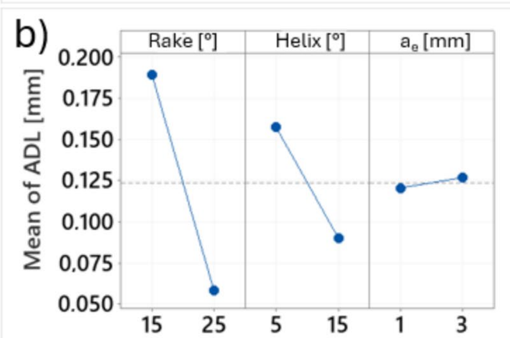

Source	DF	Adj SS	Adj MS	F-Value	P-Value
rake	1	0.03424	0.03424	37.27	**0.004**
helix	1	0.00903	0.00903	9.84	**0.035**
a_e	1	0.00008	0.00008	0.09	0.781
Error	4	0.00367	0.00091		
Total	7	0.04703			

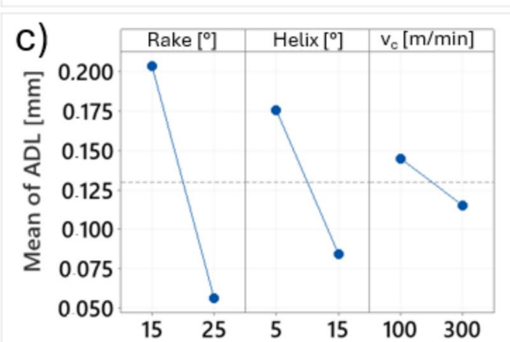

Source	DF	Adj SS	Adj MS	F-Value	P-Value
rake	1	0.04319	0.04319	19.63	**0.011**
helix	1	0.01673	0.01673	7.61	0.051
v_c	1	0.00175	0.00175	0.80	0.422
Error	4	0.00880	0.00220		
Total	7	0.07048			

Fig. 13 Investigation of control factor via ANOVA and Main effect plot for *ADL*: (**a**) f_t (v_c = 100 m/min, a_e = 3 mm) and parameters of geometry, (**b**) a_e (v_c = 100 m/min, f_t = 0.05 mm) and parameters of geometry and (**c**) v_c (a_e = 3 mm, f_t = 0.05 mm) and parameters of geometry

second most significant control factor was the rake angle This control factor was statistically stronger than v_c, radial a_e, and helix angle (see Fig. 13b and c). The high rake angle allowed to create a surface with less fibre bending or pressing the matrix under the cutting edge, meaning less burr. The helix angle was statistically significant only when compared to the a_e at the chosen significance level (see Fig. 13b). A higher helix angle helped compress both the bottom and top plies, improving the quality of the machined surface.

A direct comparison of the tested cutting tools revealed a substantial difference in machined surface quality, as measured by the ADL, between the PCD tool and all double-helix cutters; see Fig. 14. Although the double-helix cutters effectively trimmed uncut fibres and matrix, notable variations were observed among them. According to the ANOVA results, higher rake and helix angles yielded superior performance in reducing the ADL. The reduction in delamination with higher helix angle was consistent with Colligan et al. [45].

Since ADL and F had the same experimental design for a strong control factor f_t, it was possible to directly examine the relationship between these two factors. The relationship between ADL and F was expressed by the Pearson correlation method and the coefficient r. A strong correlation can be considered a correlation coefficient close to 1. In this particular case, $r = 0.447$ was calculated. The evaluated correlation was, therefore, rather moderate. The mechanism of delamination as a separation of layers is determined by the magnitude and direction of the acting forces. The results of the correlation evaluation supported this causality, but not strongly in terms of statistical significance. However, ADL increased with the resultant cutting force. The degree of correlation is graphically represented in the matrix graph (Fig. 15).

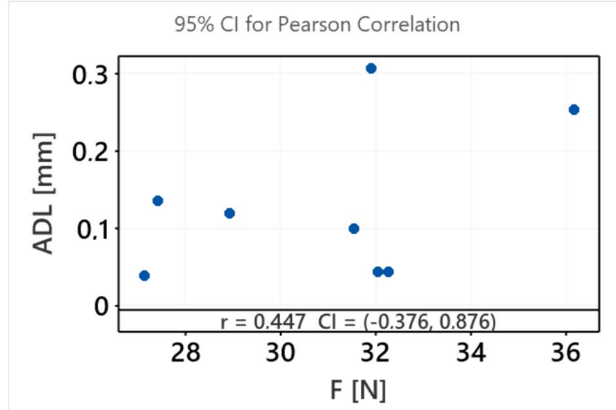

Fig. 15 Matrix plot of Temperature and ADL

3.4 Temperature

The temperature measurement method was suitable and with high repeatability. Nevertheless, the temperature was measured only on the visible surfaces and was certainly higher in the cutting zone. For this reason, the temperature was measured only for relative comparison. The PCD cutter easily removed chips from the cutting zone as is shown Fig. 16. However, the temperature of both the contact zone between cutting zone and machined surface and the chips was always high above the T_g. The less positive cutting wedge of PCD tool resulted in higher deformation accompanied by increased energy in the cutting zone and this energy was transformed to the heat.

The conditions for using a parametric ANOVA test for preliminary experiment with PCD cutter were not met and the Kruskal–Wallis test was used instead. This

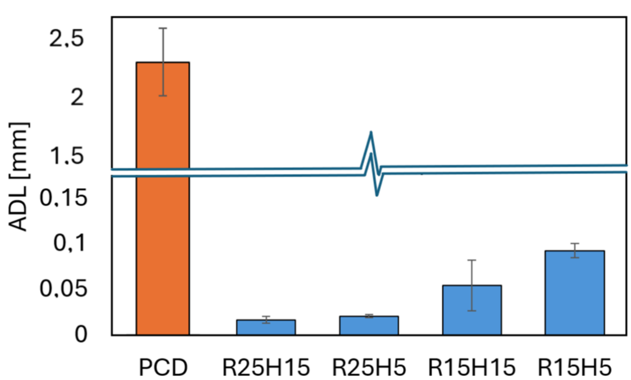

Fig. 14 Direct comparison of ADL for the tested cutter types under the cutting conditions: $a_e = 3$ mm, $f_t = 0.05$ mm, and $v_c = 100$ m/min

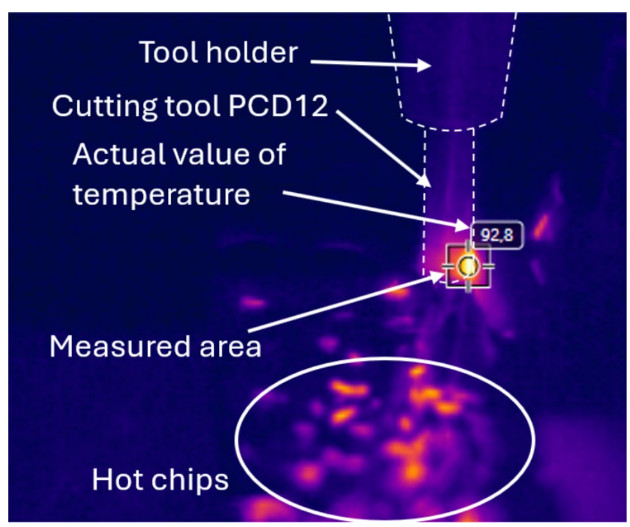

Fig. 16 Infrared image of PCD cutter during trimming

test performed for all control factors showed that feed per tooth and radial depth of cut were not statistically significant in affecting the temperature. The cutting speed had a significant influence on the temperature, with higher speeds leading to an increase in temperature (see Fig. 17). Feed per tooth was evaluated to have a decreasing effect on temperature and the opposite effect was evaluated for radial depth of cut.

The double helix cutters had grooves crossing in the middle of the cutting part. Chips were not smoothly removed from this part of the tool. It was observed that the crossing of the flutes became clogged with hot chips, leading to the gradual heating of the cutter (Fig. 18). In the second phase of the experiment was found that only v_c was statistically significant based on the 0.05 significance level. The geometry of the cutting tool did not significantly affect the temperature. The main effects plot showed that the higher the cutting speed, the higher the temperature. However, an increase in v_c by 200 m/min increased the temperature by approx. 12%, see Fig. 19. Conversely, the higher the helix angle, the lower the temperature. The rake angle had little effect on the temperature, but a higher rake angle led to higher temperatures. These results were consistent with those of our previous study [38].

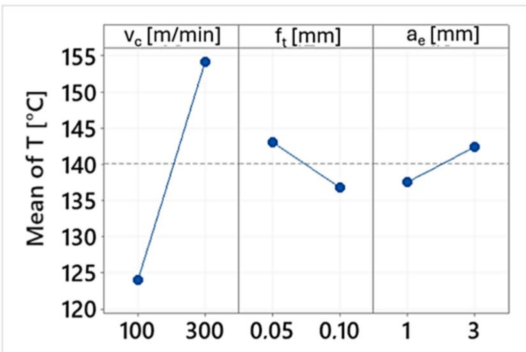

	Descriptive Statistics					Test	
	Source	n	Median	Mean Rank	Z Value	H Value	P Value
v_c	100	7	124.42	4.0	-3.24	10.50	**0.001**
	300	8	156.94	11.5	3.24		
	Overall	15		8.0			
f_t	0.05	8	144.30	9.3	1.16	1.34	0.247
	0.10	7	143.63	6.6	-1.16		
	Overall	15		8.0			
a_e	1	7	143.63	7.1	-0.69	0.48	0.487
	3	8	142.16	8.8	0.69		
	Overall	15		8.0			

Fig. 17 Investigation of control factor via Kruskal–Wallis and Main effect plot for cutting conditions control factors and *T*

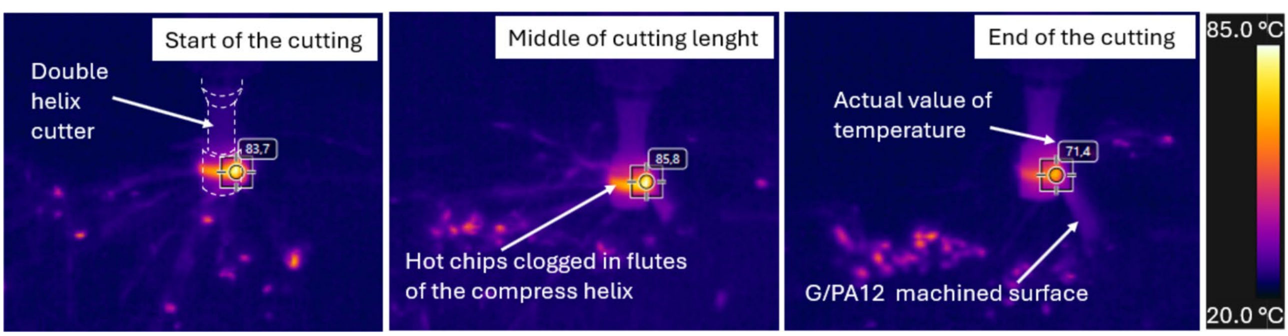

Fig. 18 An example of machining progress during trimming with compression cutter (R25H15 cutter, $v_c = 100$ m/min, $f_t = 0.05$, $a_e = 1$ mm)

Fig. 19 Investigation of control factor via ANOVA and Main effect plot for *T* and v_c ($a_e = 3$ mm, $f_t = 0.05$ mm) and parameters of geometry

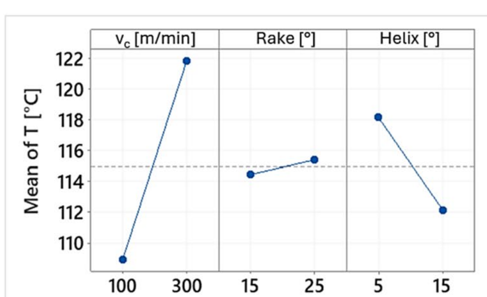

Source	DF	Adj SS	Adj MS	F-Value	P-Value
v_c	1	476.33	476.33	5.01	**0.045**
Rake	1	16.06	16.06	0.17	0.688
Helix	1	80.32	80.32	0.85	0.376
Error	12	1140.3	95.02		
Lack-of-Fit	4	1032.3	258.08	19.12	0.000
Pure Error	8	107.96	13.50		
Total	15	1713.0			

The PCD cutter generated more heat during milling than any of the double-helix cutters, likely due to its low rake angle, which causes increased deformation during chip formation, see Fig. 20. However, the limited capacity of the double-helix design to evacuate chips, particularly at the middle section of the compression helix, also contributes to heat generation. As a result, the temperature difference between the PCD and double-helix cutters was not as large as one might expect if the rake angle were the only contributing factor.

For this experiment, ADL was measured as well. The effect of temperature on ADL was also demonstrated using correlation analysis using the same method as in the previous case. The correlation was expressed as the correlation coefficient r. For the measured T and ADL, $r = 0.290$ — a weak to moderate correlation. Temperature had only a limited effect on ADL. The degree of correlation and increasing ADL with temperature is graphically represented in the matrix plot (Fig. 21).

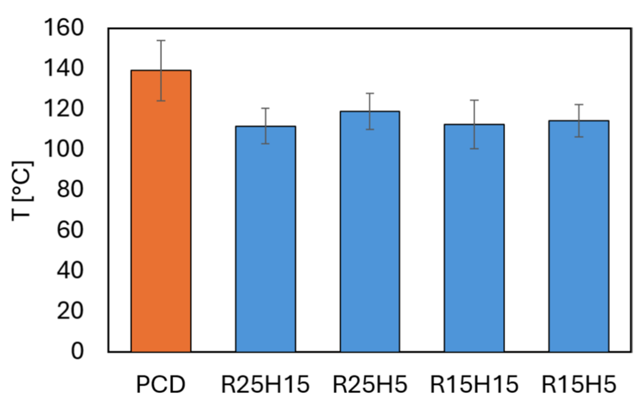

Fig. 20 Direct comparison of T for the tested cutter types under the cutting conditions: $a_e = 3$ mm, $f_t = 0.05$ mm, and $v_c = 100$ m/min

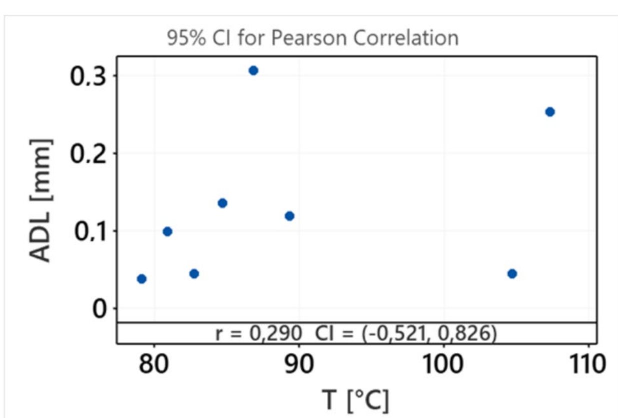

Fig. 21 Matrix plot of Temperature and ADL

4 Conclusion

The primary challenge encountered when milling G/PA12 composites is achieving a high-quality machined surface. Selecting an appropriate cutting tool and optimizing cutting conditions are essential to meeting surface finish requirements. This study employed a statistical approach to identify significant control factors, namely tool geometry and cutting conditions, and to evaluate their influence on cutting forces, temperature, and surface quality. The key findings are as follows:

- Cutting forces are significantly affected by the feed per tooth and radial depth of cut. Cutting conditions exerted a more pronounced influence on the resultant cutting force than tool geometry.
- The resultant cutting force was higher for double-helix cutters compared to the PCD cutter, likely due to the increased number of teeth engaged and more difficult chip evacuation.
- A cutting force model that incorporates geometric aspects of the double-helix cutter was developed. Within the tested parameter range, it demonstrated an excellent coefficient of determination ($R^2 = 0.994$), enabling reliable prediction of cutting forces when milling G/PA12.
- Effective cutting of uncut fibres and matrix required a positive compress geometry in the double-helix cutter. In contrast, the PCD tool, which lacked this geometry, produced up to 100 times higher ADL values (depending on the rake angle).
- Feed per tooth emerged as the most significant control factor influencing the ADL; higher feed rates created lower ADL values. Rake angle also affected surface quality, although to a slightly greater extent than the helix angle.
- The emissivity of G/PA12 for infrared camera measurements was established as 0.89.
- The cutting temperature, as measured by infrared camera, consistently exceeded the matrix's glass transition temperature but did not adversely affect the machining process.
- Owing to their positive geometry, the double-helix cutters reduced cutting temperature by up to 20% compared to the PCD cutter.
- Cutting speed proved to be the most critical control factor for temperature management. Should any issues arise during G/PA12 machining, reducing the cutting speed is strongly recommended.
- The moderate correlation was observed between the resultant force and ADL and between temperature and ADL. ADL increased with both temperature and machining forces. The relationship expressed by the correlation coefficient was stronger for forces and ADL than for temperature and ADL.

This study lays a foundation for milling G/PA12 composites and offers strategies to address the main challenges associated with this thermoplastic composite reinforced with woven glass fibres. Future investigations may further refine these findings by examining more detailed relationships among control factors, delamination, and temperature, thereby enhancing both quality and productivity in G/PA12 machining.

Acknowledgements The authors acknowledge the support from the ESIF, EU Operational Programme Research, Development and Education, and from the Center of Advanced Aerospace Technology (CZ.02.1.01/0.0/0.0/16_019/0000826), Faculty of Mechanical Engineering, Czech Technical University in Prague and *National Centre of Competence in ENGINEERING* (TN01000015), which is co-financed from the state budget by the Technology agency of the Czech Republic under the National Centre of Competence Programme.

Author contribution Petr Mašek: Methodology, Writing, Visualization, Editing, Data acquisition, Data analysis, Jaroslav Kovalčík: Writing—review & editing, Data analysis, Visualisation. Pavel Zeman: Writing—review & editing, Resources.

Funding Open access publishing supported by the institutions participating in the CzechELib Transformative Agreement. This publication was created with the contribution of the knowledge obtained within the project, Development and Education, and from the *Center of Advanced Aerospace Technology* Reg. No CZ. 02.1.01/0.0/0.0/16_019/0000826.

This work was created also within the project *National Centre of Competence in ENGINEERING* (TN01000015), which is co-financed from the state budget by the Technology agency of the Czech Republic under the National Centre of Competence Programme.

Declarations

Competing interests The authors declare that they have no known competing financial interests or personal relationships that could have appeared to influence the work reported in this paper.

References

1. Harris B (1999) Engineering composite materials. The Institute of Metals, London
2. Mangalgiri P (1999) Composite materials for aerospace applications. Bull Mater Sci 22:657–664. https://doi.org/10.1007/BF02749982
3. Geier N, Davim JP, Szalay T (2019) Advanced cutting tools and technologies for drilling carbon fibre reinforced polymer (CFRP) composites: a review. Composites Part A 125:105552. https://doi.org/10.1016/j.compositesa.2019.105552
4. Vilis J, Vitek R, Zouhar J, Stejskal M, Neumann V (2023) Experimental investigation of armour (Armox-Aramid-UHMWPE). Manuf Technol 1:14. https://doi.org/10.21062/mft.2023.083
5. Davies-Frey D, Bowkett M, Constatnt E, Thanapalan K (2020) Failure detection of composite materials in sport applications. In: 2020 7th International Conference on Control, Decision and Information Technologies (CoDIT) Prague. https://doi.org/10.1109/CoDIT49905.2020.9263966
6. Teti R (2002) Machining of composite materials. CIRP Ann Manuf Technol 51(2):611–634. https://doi.org/10.1016/S0007-8506(07)61703-X
7. Sheikh-Ahmad JY (2009) Machining of polymer composites. Springer Science + Business Media, New York
8. Hocheng H, Puw HY (1993) Machinability of fiber-reinforced thermoplastic in drilling. J Eng Mater Technol 115:146–149. https://doi.org/10.1115/1.2902148
9. Ge J, Catalanotti G, Falzon B, Higgins C et al (2024) Process characteristics, damage mechanisms and challenges in machining of fibre reinforced thermoplastic polymer (FRTP) composites: a review. Composites Part B: Eng 273:111247. https://doi.org/10.1016/j.compositesb.2024.111247
10. Ciecielag K (2024) Influence of the cooling method on cutting force and recurrence analysis in polymer composite milling. Materials 17:5981. https://doi.org/10.3390/ma17235981
11. Sambruno A, Bañon F, Salguero J et al (2021) Study of milling of low thickness thermoplastic carbon fiber composites in function of tool geometry and cutting conditions. Int J Adv Manuf Technol 114:2515–2526. https://doi.org/10.1007/s00170-021-07050-1
12 Mašek P, Zeman P, Kolář P (2013) Development of cutting tool for composites with thermoplastic matrix. MMScience 2013:422–42. https://doi.org/10.17973/MMSJ.2013_10_201312
13. Davim JP (2009) Machining composite materials London: ISTE Ltd
14. Azmi A (2013) Chip formation studies in machining fibre reinforced polymer composites. Int J Mater Prod Technology 1:32–46. https://doi.org/10.1504/IJMPT.2013.052790
15. Puw HY, Hocheng H (1993) Machinability test of carbon fiber-reinforced plastics in milling. Mater Manuf Processes 8(6):717–729. https://doi.org/10.1080/10426919308934875
16. Mazumder MJ, Chang RJ, Bond RL (1982) Aerodynamic and morphological properties of carbon-fiber aerosols. Aerosol Sci Technol 1(4):427–440. https://doi.org/10.1080/02786828208958606
17. Ge J, Catalanotti G, Falzon G, McClelland J, Higgins C, Jin Y, Sun D (2022) Towards understanding the hole making performance and chip formation mechanism of thermoplastic fibre/polyetherketoneketone compossite. Composites Part B 234:109752. https://doi.org/10.1016/j.compositesb.2022.109752
18. Rahman M, Ramakrishnan S, Thoo HC (1999) Machinability study of carbon/PEEK composites. Mach Sci Technol 3(1):49–59. https://doi.org/10.1080/10940349908945682
19. Ehrenstein GW (2009) Polymerní kompozitní materiály. Praha: Scientia
20. He Y, Qing H, Zhang S, Wang D, Zhu S (2017) The cutting force and defect analysis in milling of carbon. Int J Adv Manuf Technol 93:1829–1842. https://doi.org/10.1007/s00170-017-0613-6
21. Patel P, Chaudhary V, Patel K, Gohil P (2018) Milling of polymer matrix composites: a review. Int J Appl Eng Res 13(10):7455–7465
22. Hintze W, Brügmann F (2018) Influence of spatial tool inclination on delamination when milling CFRP. J Mater Process Technol 252:830–837. https://doi.org/10.1016/j.jmatprotec.2017.10.041
23. Davim JP, Reis P (2005) Demage and dimensional precision on milling carbon fiber-reinforced plastics using design experiment.

J Mater Process Technol 160:160–167. https://doi.org/10.1016/j.jmatprotec.2004.06.003
24. Davim JP, Reis P, Antonio CC (2004) A study on milling of galss fiber reinforced plastics manufactured by hand-lay up using statistical analysis (ANOVA). Compos Struct 64(493):500. https://doi.org/10.1016/j.compstruct.2003.09.054
25. Geiger N, Xu J, Poór D, Dege J, Davim JP (2023) A review on advance cutting tools and technologies for ege trimming of carbon fibre reinforced polymer (CFRP) composites. Compos Part B: Eng 266:111037. https://doi.org/10.1016/j.compositesb.2023.111037
26. Vavruška P, Pešice M, Zeman P, Kozlok T (2022) Automated feed rate optimization with consideration of angular velocity according to workpiece shape. Results Eng 16:100762. https://doi.org/10.1016/j.rineng.2022.100762
27. Praveen R, Perumal AE (2010) Taguchi Analysis of surface roughness and delamination associated with various cemented carbide K10 end mills in milling of GFRP. J Eng Sci Technol 3(1):58–64. https://doi.org/10.25103/jestr.031.11
28. Jenarthanan MP, Naresh N (2015) Process parameters optimization on machining force and delamination factor in milling of GFRP composite using gray relational analysis. Indian J Eng Mater Sci 22:313–320
29. Jenarthanan MP, Nishanth G, Bharatwaj R (2016) Optimization of machining parameters in end milling of GFRP composites based on the Taguchi method with fuzzy logics. Int J Knowl –based Intel Eng Syst 20(3):123–134. https://doi.org/10.3233/KES-160338
30. Voss R, Seeholzer L, Kuster F, Wegener K (2017) Influence of fibre orientation, tool geometry and process parameters on surface quality in milling of CFRP. CIRP J Manuf Sci Technol 18:75–91. https://doi.org/10.1016/j.cirpj.2016.10.002
31. Zenia S, Ben Ayed I, Nouari M, Delameziere A (2015) Numerical analysis of the interaction between the cutting forces, induced cutting damage, and machining parameters of CFRP composites. Int J Adv Manuf Techno 78:465–480. https://doi.org/10.1007/s00170-014-6600-2
32. Sheikh-Ahmad J, El-Hofy M, Almaskari F, Kerrigan K, Takikaw Y (2019) The evolution of cutting forces during slot milling of unidirectional carbon fiber reinforced polymer (UD-CFRP) composites. Procedia CIRP 85:127–132. https://doi.org/10.1016/j.procir.2019.09.043
33. Chatelain J-F, Zaghbani I (2012) A comparison of special helical cutter geometries based on cutting forces for the trimming of CFRP laminates. Int J Mech 6(1):51–59
34. Su F, Yuan J, Sun F, Wang Z, Deng Z (2018) Modeling and simulation of milling forces in milling plain woven carbon fibre-reinforced plastic. Int J Adv Man Tech 95:4141–4152. https://doi.org/10.1007/s00170-017-1556-7
35. Kalla D, Sheikh-Ahmad J, Twomey J (2010) Prediction of cutting forces in helical end milling fiber reinforced polymers. Int J Mach Tools Manuf 50:882–891. https://doi.org/10.1016/j.ijmachtools.2010.06.005
36. Altintas Y (2000) Manufacturing automation, Cambridge: the press syndicate of the university of cambridge. https://doi.org/10.1017/CBO9780511843723
37. Karpat Y, Polat N (2013) Mechanistic force modeling for milling of carbon fiber reinforced polymers with double helix tools. CIRP Ann Manuf Technol 62:95–98. https://doi.org/10.1016/j.cirp.2013.03.105
38. Mašek P, Zeman P, Kolář P, Holešovský F (2019) Edge trimming of C/PPS plates. Int J Adv Manuf 101:157–170. https://doi.org/10.1007/s00170-018-2857-1
39. Kerrigan K, Thil J, Hewison R et al (2012) An integrated telemetric thermocouple sensor for process monitoring of CFRP milling operations. 5th CIRP Conference on High Performance Cutting 2012. https://doi.org/10.1016/j.procir.2012.04.080
40. Yoshiro T, Ogawa T, Sasahara H (2013) Temperature measurement of cutting tool and machined surface layer in milling of CFRP. Int J Mach Tools Manuf 70:63–69. https://doi.org/10.1016/j.ijmachtools.2013.03.009
41. Jia Z, Fu R, Quan B, He C (2016) Temperature effects in end milling carbon fiber reinforced polymer composites. Polym Compos 39(2):437–447. https://doi.org/10.1002/pc.23954
42. ISO 3002–4:1984 (1984) Basic quantities in cutting and grinding Part 4: forces, energy, power
43. Wyatt C (1978) CHAPTER IV - blackbody radiation. Radiometric calibration: theory and methods. Academic Press
44. Sorrentino L, Turchetta S (2011) Milling of carbon fiber-reinforced plastic: analysis of cutting forces and surface roughness. 18th internationl conference on composite materials. https://iccm-central.org/Proceedings/ICCM18proceedings/papers/F13-2-AF1404.pdf
45. Colligan K, Ramulu M (1991) Delamination in surface plies of graphite/epoxy caused by the edge trimming process. Washington: PED-CPů.49/MD-Vol.27, Processing and manufacturing of composite materials - ASME. https://ui.adsabs.harvard.edu/abs/1991pmcm.proc..113C